IOP Publishing Physica Scripta
Phys. Scr. 95 (2020) 035002 (12pp) https://doi.org/10.1088/1402-4896/ab4cac

Shape effects of molybdenum disulfide (nm) micro-rotating particles in crosswise transport of hydrogen oxide: (MoS_2–H_2O) nano polymer gel

M S Alqarni[1,3], R Tabassum[2], M Y Malik[1] and R Mehmood[2,3]

[1] Department of Mathematics, College of Science, PO Box 9004, King Khalid University, Abha 61413, Saudi Arabia
[2] Department of Mathematics, Faculty of Natural Sciences, HITEC University, Taxila Cantt, Pakistan

E-mail: msalqarni@kku.edu.sa and rashid.mehmood@hitecuni.edu.pk

Received 30 May 2019, revised 16 September 2019
Accepted for publication 10 October 2019
Published 4 February 2020

Abstract

Nano polymers have emerged as a new development offering promising durability, anti-corrosion and thermal efficiency. Nanoparticles shape, size and volume fraction plays critical part in improved performance of heat exchanger systems involving modern manufacturing processes of nano-rheological materials. Molybdenum Disulfide nanostructures finds significant applications in desulfurization processes, in thermoelectric appliances and many more. Motivated by elaborating in further detail, the present article presents a mathematical and computational study on steady, two-dimensional, non-aligned thermo-fluid transport of Molybdenum Disulfide doped-Hydrogen oxide (H_2O) based micropolar fluid. To simulate real nano polymer dynamics, the Tiwari-Das model for nano particle concentration and Maxwell-Garnet model for nanofluid thermal conductivity is exploited. The conservation equations for mass, momentum (normal and tangential) and energy are normalized by employing suitable transformations. Numerical solutions are attained via Keller Box method in MATLAB symbolic software. The impact of key emerging dimensionless parameter i.e. nanoparticles volume fraction (ϕ) and various shape effects of molybdenum disulfide nanoparticles on non-dimensional normal and tangential velocity components, micro rotation profile, temperature, shear stress at the wall and local heat flux is explored graphically. Local heat flux and micro-rotation profile is boosted while tangential skin friction coefficient depletes with the insertion of blade shaped nanoparticles. Moreover greatest thermal conductivity is achieved with the insertion of blade shape nanoparticles.

Keywords: molybdenum disulfide, shape factor, micro rotation, crosswise flow, Keller box

(Some figures may appear in colour only in the online journal)

1. Introduction

Nano-technology has had an insightful impact on countless technologies comprising aircraft components, rocket propulsion, medicine and also renewable energy systems. Today nano-technology is the best prospect for clean inexpensive power systems. Although there is a noteworthy progress in refining working fluids by nano-particle doping, only very recently have scientists focused on exploring the shape effects of nanoparticles in such processes.

This environmentally-friendly flexible polymeric sheets that are precision-designed to contain a nano-particle fluid that is essentially water-based paint.

Molybdenum Disulfide nanostructures are gaining substantial consideration because of their potential applications as catalysts for desulfurization processes, thermoelectric

[3] Authors to whom any correspondence should be addressed.

appliances, electronic devices especially in field effect transistors. Molybdenum Disulfide nanoparticles are more prone to chemical reaction and friction. Like graphite, it is commonly used as a solid lubricant due to its low friction characteristics and robustness. The insertion of nano sized particles to the base fluid, introduced by Choi [1] not only enhances the thermal conductivity but also considerably affect the viscosity of fluid. Properties of nanofluid flow significantly depend upon several aspects including shape, size, volume fraction and material of nanoparticles etc. Spherical and non-spherical shapes of nanoparticles possess higher thermal conductivity compare to base fluids and are therefore extremely useful in several engineering and industrial processes. Traditionally cylindrical shaped nanoparticles are used in many researches. Thermo-physical properties of nanofluid are significantly influenced by various shapes nanoparticles. There are very few studies related to nanoparticles shape effects on fluid flow with different geometries and flow properties. Timofeeva *et al* [2] examined the influence of diverse forms of alumina nanoparticles on water and ethylene glycol nanofluid flow characteristics. Their investigation showed that the thermal conductivity reduces for sphericity values less than 0.6 of alumina particles. They also noticed that viscosity of the flow was highly influenced by surface charge of nanoparticles. Ellahi *et al* [3] scrutinized natural convection and shape effects of copper nanoparticles on entropy generation along an inverted cone using Hamilton–Crosser model. In their study, entropy generation analysis was performed for Copper nanoparticles. Their notable findings include that the highest fluid deceleration for the case of brick shaped Copper particles. Also particle friction and viscous dissipation contributed in boosting surface skin friction. Shafie *et al* [4] investigated shape effects of MoS_2 nanoparticles in water within a permeable channel by considering mixed convection and radiation effects. An oscillatory wall is considered in the geometry of flow and results were calculated through perturbation method. They found highest viscosity and thermal conductivity with cylindrical and platelet shaped nanoparticles. Hiemenz [5] addressed the dynamics of stagnation point flow. Wang and Mujumdar [6] explored mixed convective nanofluid thermal characteristics. Nadeem *et al* [7] considered transverse stagnated second grade fluid near an extending surface. Brownian motion and thermophertic effects were considered in their analysis. They investigated analytically the flow transport, heat transfer and concentration profile through HAM. It was found that fluid elasticity had increasing effect on velocity of the flow at a point. Blood flow analysis using Jeffery nanofluid has been performed by Nadeem *et al* [8]. Influence of gravity was taken into account due to vertical mounting direction of tube. Heat generation along with chemical reaction effects on nanofluid over a convective plate submerged in a absorptive medium were explored by Rashidi *et al* [9] and concluded that Nusselt number elevates with reaction constant and Lewis number while it is decreases with chemical reaction and generation constants. Casson fluid flow with addition of nanoparticles was inspected by Mehmood *et al* [10]. They inspected influence of nanoparticles concentration on heat flux. The obtained results revealed that Casson fluid parameter depletes the fluid velocity. Rashidi *et al* [11] employed OHAM to study surface slip effects on convective flow of a nanofluid. Aziz *et al* [12] examined the rotating fluid with thermal slip condition. They portrayed Bejan number to present entropy generation. It was discovered that nanofluid caused more entropy as compared pure fluid, moreover maximum entropy was produced when nanoparticles of gold were suspended in fluid. Rashid *et al* [13] deliberated water and Ethylene-Glycol nanofluid over a stretched sheet. Ethylene-Glycol based fluid proved to be promising in terms of rapid heat flux. Rana *et al* [14] analyzed oblique slip flow of a chemically reactive Casson fluid. Their key findings included that the slip parameter plays vital role in lowering chemical spices concentration on surface. Micropolar fluid model effectively describes rheological fluids undergoing micro-rotation. Typical examples of such fluids include polymer extracts, platelets, smoky clouds, suspensions and liquid crystals. Eringen [15] presented a comprehensive insight of micropolar fliuds. Nazar *et al* [16] examined steady incompressible flow of micropolar fluid. Computational analysis was made through Keller-box algorithm. Effect of chemical reaction on natural convective micropolar fluid was explored by Damesh *et al* [17]. Micropolar fluid flow with nanoparticles over a moving cylinder was deliberated by Nadeem *et al* [18]. Similarly Rehman and Nadeem [19] inspected micropolar fluid over a vertical cylinder. Hydromagnetic slip flow by considering micro rotation has been investigated by Mahmoud and Waheed [20]. Impact of copper and silver nanoparticles on micropolar fluid has been discovered by Hussain *et al* [21]. Sheikholeslami *et al* [22] studied micropolar fluid channel flow in presence of chemical reaction. They compared analytical HPM and numerical results obtained by R K method of fourth order. It was suggested that Peclet and Reynolds numbers are directly related with Sherwood and Nusselt numbers for the case of suction as well as injection. Hashim *et al* [23] examined mixed convective micropolar nanofluid stagnated flow along vertically stretched sheet. Adegbie *et al* [24] investigated the stagnated flow of micropolar fluid on a horizontal surface stretched linearly. It was projected that oblique flow velocity of micropolar fluid over melting surface can be enhanced by adopting variable properties of fluid. They examined variable thermal conductivity and viscosity effects on a micropolar fluid. Mehmood *et al* [25] used OHAM to solve the flow problem of rotating micropolar fluid through a pair of parallel plates. Waqas *et al* [26] investigated the MHD micropolar fluid towards an extended surface with mixed convection. Some more related studies can be found in [27–36]. This communication addresses steady two dimensional oblique transport of micropolar nanofluid towards a stretching sheet. Such a simulation, although greatly relevant to nano-polymer manufacturing processes has not thus far received any attention in the literature. Various shape effects of molybdenum disulphide nanoparticles on flow and heat transfer characteristics are explored and analyzed. Four different shapes of MoS_2 namely Brick, Blade, Cylinder and Platelets doped in hydrogen oxide based fluid are considered in our analysis

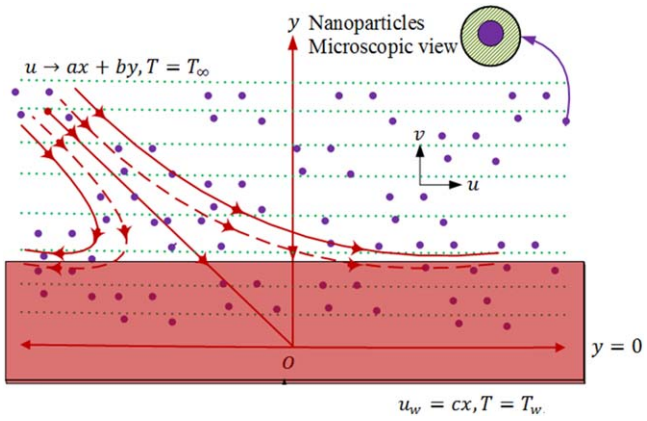

Figure 1. Physical description of the problem.

Table 1. Constant A and B [29].

Model	Brick	Blade	Cylinder	Platelet
A	1.9	14.6	13.5	37.1
B	471.4	123.3	904.4	612.6

(See Table 1). It is envisaged that the current effort will provide a good compliment to experimental and more complex computational fluid dynamics simulations of nano-polymer coating synthesis.

2. Physical modeling and empirical relations

Let us deliberate the transverse incompressible flow of micropolar fluid in which molybdenum disulfide nanoparticles are injected. Two equal but oppositely directed forces are used on surface in such a way that origin remains fixed as shown in figure 1. Model equations for the flow phenomena under consideration are:

$$\frac{\partial \hat{u}^*}{\partial \hat{x}^*} + \frac{\partial \hat{v}^*}{\partial \hat{y}^*} = 0, \tag{1}$$

$$\hat{\rho}_{\rm nf}\left(\hat{u}^*\frac{\partial \hat{u}^*}{\partial \hat{x}^*} + \hat{v}^*\frac{\partial \hat{u}^*}{\partial \hat{y}^*} + \frac{1}{\hat{\rho}_{\rm nf}}\frac{\partial \hat{p}^*}{\partial \hat{x}^*}\right) = (\hat{\mu}_{\rm nf} + \hat{k})\frac{\partial^2 \hat{u}^*}{\partial \hat{y}^{*^2}} + \hat{k}\frac{\partial \hat{N}^*}{\partial \hat{y}^*}, \tag{2}$$

$$\hat{\rho}_{\rm nf}\left(\hat{u}^*\frac{\partial \hat{v}^*}{\partial \hat{x}^*} + \hat{v}^*\frac{\partial \hat{v}^*}{\partial \hat{y}^*} + \frac{1}{\hat{\rho}_{\rm nf}}\frac{\partial \hat{p}^*}{\partial \hat{y}^*}\right) = (\hat{\mu}_{\rm nf} + \hat{k})\frac{\partial^2 \hat{v}^*}{\partial \hat{y}^{*2}} - \hat{k}\frac{\partial \hat{N}^*}{\partial \hat{x}^*}, \tag{3}$$

$$\hat{\rho}_{\rm nf} j\left(\hat{u}^*\frac{\partial \hat{N}^*}{\partial \hat{x}^*} + \hat{v}^*\frac{\partial \hat{N}^*}{\partial \hat{y}^*}\right) = -\hat{k}\left(2\hat{N}^* + \frac{\partial \hat{u}^*}{\partial \hat{y}^*}\right) + \hat{\gamma}_{\rm nf}\frac{\partial^2 \hat{N}^*}{\partial \hat{y}^{*^2}}, \tag{4}$$

Table 2. Sphericity for different shapes of nanoparticles [29].

Model	Brick	Blade	Cylinder	Platelet
ω	0.81	0.36	0.62	0.52

$$\hat{u}^*\frac{\partial \hat{T}^*}{\partial \hat{x}^*} + \hat{v}^*\frac{\partial \hat{T}^*}{\partial \hat{y}^*} = \hat{\alpha}^*_{\rm nf}\frac{\partial^2 \hat{T}^*}{\partial \hat{y}^{*^2}}. \tag{5}$$

Here, $\hat{u}^*$, $\hat{v}^*$ are components of velocity along $\hat{x}^*$, $\hat{y}^*$ directions, $\hat{p}^*$ stands for pressure, $\hat{\rho}_{\rm nf}$ denote density and $\hat{\alpha}^*_{\rm nf} = \frac{\hat{k}_{\rm nf}}{(\hat{\rho}c_{\hat{p}})_{\rm nf}}$ denote nano fluid effective thermal diffusivity. $\hat{N}^*$ symbolizes the micro-rotation. $\hat{T}^*$ denotes temperature, ϕ is nanoparticles volumetric fraction, $\hat{k}$ represent vortex viscosity, $\hat{\gamma}_{\rm nf} = \left(\hat{\mu}_{\rm nf} + \frac{\hat{k}}{2}\right)j$ represent spin gradient viscosity, $j = \frac{\hat{v}_f}{c}$ refer to micro-inertia density and $\hat{\mu}_{\rm nf}$ stands for nanofluid dynamic viscosity. Effective nano fluid density $\hat{\rho}_{\rm nf}$ and capacitance $(\hat{\rho}c_{\hat{p}})_{\rm nf}$ are defined as [27]

$$\hat{\rho}_{\rm nf} = (1 - \phi)\hat{\rho}_f + \phi\hat{\rho}_s, \tag{6}$$

$$(\hat{\rho}c_{\hat{p}})_{\rm nf} = (1 - \phi)(\hat{\rho}c_{\hat{p}})_f + \phi(\hat{\rho}c_{\hat{p}})_s, \tag{7}$$

where, $\hat{\rho}_s$ and $\hat{\rho}_f$ represent nanoparticles and water density respectively. In the present investigation the effective thermal conductivity $\hat{k}_{\rm nf}$ can be estimated as [28]

$$\frac{\hat{k}_{\rm nf}}{\hat{k}_f} = \frac{\hat{k}_s + (m-1)\hat{k}_f + (m-1)(\hat{k}_s - \hat{k}_f)\phi}{\hat{k}_s + (m-1)\hat{k}_f - \phi(\hat{k}_s - \hat{k}_f)}, \tag{8}$$

where, $\hat{k}_f$ and $\hat{k}_s$ signify the thermal conductivities of water as base fluid and molybdenum disulphide. Empirical shape factor defined as $m = \frac{3}{\omega}$, where ω denotes the sphericity factor. Accordingly the dynamic viscosity is given by

$$\hat{\mu}_{\rm nf} = \hat{\mu}_f(1 + A\phi + B\phi^2), \tag{9}$$

where, A and B are constants depending upon the particle shape. Their values are given below

Sphericity values for various nanoparticles shapes are expressed in table 2.

Thermo-physical characteristics of H_2O and molybdenum are

Pertinent boundary conditions as

$$\hat{u}^* = c\hat{x}^*,\ \hat{v}^* = 0,\ \hat{N}^* = -n\frac{\partial \hat{u}^*}{\partial \hat{y}^*},\ \hat{T}^* = \hat{T}_w \text{ at } \hat{y}^* = 0, \tag{10}$$

$$\hat{u}^* = a\hat{x}^* + b\hat{y}^*,\ \hat{N}^* = \text{constant},\ \hat{T}^* = \hat{T}_\infty \text{ when } \hat{y}^* \to \infty, \tag{11}$$

where a, b and c are invariant, $\hat{T}_\infty$ stands for ambient temperature and $\hat{T}_w$ denote wall temperature. Moreover, n symbolizes microelements concentration [16].

Introducing following appropriate transformations:

$$\hat{x} = \hat{x}^*\sqrt{\frac{c}{\hat{\nu}_f}},\ \hat{y} = \hat{y}^*\sqrt{\frac{c}{\hat{\nu}_f}},\ \hat{u} = \hat{u}^*\frac{1}{\sqrt{\hat{\nu}_f c}},\ \hat{v} = \hat{v}^*\frac{1}{\sqrt{\hat{\nu}_f c}},$$
$$\hat{p} = \frac{\hat{p}^*}{(\hat{\rho}\hat{\nu})_f c},\ \hat{T} = \frac{\hat{T}^* - \hat{T}_\infty}{\hat{T}_w - \hat{T}_\infty},\ \hat{N} = \frac{\hat{N}^*}{c}, \tag{12}$$

where, $\hat{\nu}_f$ denote base fluid effective kinematic viscosity. Invoking equation (11), the equations (1)–(5), (10), (11) in non-dimensional form are

$$\frac{\partial \hat{u}}{\partial \hat{x}} + \frac{\partial \hat{v}}{\partial \hat{y}} = 0, \tag{13}$$

$$\hat{u}\frac{\partial \hat{u}}{\partial \hat{x}} + \hat{v}\frac{\partial \hat{u}}{\partial \hat{y}} + \frac{\hat{\rho}_f}{\hat{\rho}_{\rm nf}}\frac{\partial \hat{p}}{\partial \hat{x}} = \frac{\hat{\rho}_f}{\hat{\rho}_{\rm nf}}(1 + A\phi + B\phi^2 + K)\frac{\partial^2 \hat{u}}{\partial \hat{y}^2} + \frac{\hat{\rho}_f}{\hat{\rho}_{\rm nf}}K\frac{\partial \hat{N}}{\partial \hat{y}}, \tag{14}$$

$$\hat{u}\frac{\partial \hat{v}}{\partial \hat{x}} + \hat{v}\frac{\partial \hat{v}}{\partial \hat{y}} + \frac{\hat{\rho}_f}{\hat{\rho}_{\rm nf}}\frac{\partial \hat{p}}{\partial \hat{y}} = \frac{\hat{\rho}_f}{\hat{\rho}_{\rm nf}}(1 + A\phi + B\phi^2 + K)\frac{\partial^2 \hat{v}}{\partial \hat{y}^2} - \frac{\hat{\rho}_f}{\hat{\rho}_{\rm nf}}K\frac{\partial \hat{N}}{\partial \hat{x}}, \tag{15}$$

$$\hat{u}\frac{\partial \hat{N}}{\partial \hat{x}} + \hat{v}\frac{\partial \hat{N}}{\partial \hat{y}} = -K\frac{\hat{\rho}_f}{\hat{\rho}_{\rm nf}}\left(2\hat{N} + \frac{\partial \hat{u}}{\partial \hat{y}}\right) + \frac{\hat{\rho}_f}{\hat{\rho}_{\rm nf}} \times \left(1 + A\phi + B\phi^2 + \frac{K}{2}\right)\frac{\partial^2 \hat{N}}{\partial \hat{y}^2}, \tag{16}$$

$$\hat{u}\frac{\partial \hat{T}}{\partial \hat{x}} + \hat{v}\frac{\partial \hat{T}}{\partial \hat{y}} = \frac{\hat{\alpha}_{\rm nf}}{\hat{\nu}_f}\frac{\partial^2 \hat{T}}{\partial \hat{y}^2}, \tag{17}$$

$$\hat{u} = \hat{x},\ \hat{v} = 0,\ \hat{N} = -n\frac{\partial \hat{u}}{\partial \hat{y}},\ \hat{T} = 1 \text{ at } \hat{y} = 0, \tag{18}$$

$$\hat{u} = \frac{a}{c}\hat{x} + \frac{b}{c}\hat{y},\ \hat{N} = -\frac{b}{c},\ \hat{T} = 0 \text{ when } \hat{y} \to \infty, \tag{19}$$

where, $K = \frac{\hat{k}}{\hat{\mu}_f}$ stands for micropolar coupling parameter. Incorporating stream function relations as [8]

$$\hat{u} = \frac{\partial \psi}{\partial \hat{y}},\ \hat{v} = -\frac{\partial \psi}{\partial \hat{x}}. \tag{20}$$

Using equation (20) in equations (13)–(19) and considering $\hat{p}_{\hat{x}\hat{y}} = \hat{p}_{\hat{y}\hat{x}}$ in equations (14) and (15), we have

$$\frac{\hat{\rho}_f}{\hat{\rho}_{\rm nf}}(1 + A\phi + B\phi^2 + K)\frac{\partial^2}{\partial \hat{y}^2}(\nabla^2\psi) + \frac{\hat{\rho}_f}{\hat{\rho}_{\rm nf}}K\nabla^2\hat{N} + \frac{\partial(\psi, \nabla^2\psi)}{\partial(\hat{x}, \hat{y})} = 0, \tag{21}$$

$$\frac{\partial \psi}{\partial \hat{y}}\frac{\partial \hat{N}}{\partial \hat{x}} - \frac{\partial \psi}{\partial \hat{x}}\frac{\partial \hat{N}}{\partial \hat{y}} = -K\frac{\hat{\rho}_f}{\hat{\rho}_{\rm nf}}\left(2\hat{N} + \frac{\partial^2 \psi}{\partial \hat{y}^2}\right) + \frac{\hat{\rho}_f}{\hat{\rho}_{\rm nf}} \times \left(1 + A\phi + B\phi^2 + \frac{K}{2}\right)\frac{\partial^2 \hat{N}}{\partial \hat{y}^2}, \tag{22}$$

$$Pr\left(\frac{\partial \psi}{\partial \hat{y}}\frac{\partial \hat{T}}{\partial \hat{x}} - \frac{\partial \psi}{\partial \hat{x}}\frac{\partial \hat{T}}{\partial \hat{y}}\right) = \frac{\hat{\alpha}_{\rm nf}}{\hat{\alpha}_f}\frac{\partial^2 \hat{T}}{\partial \hat{y}^2}, \tag{23}$$

where $Pr = \frac{\hat{\nu}_f}{\hat{\alpha}_f}$ is termed as Prandtl number. Associated boundary conditions are

$$\psi = 0,\ \frac{\partial \psi}{\partial \hat{y}} = \hat{x},\ \hat{N} = -n\frac{\partial^2 \psi}{\partial \hat{y}^2},\ \hat{T} = 1,\ \text{at } \hat{y} = 0, \tag{24}$$

$$\psi = \frac{a}{c}\hat{x}\hat{y} + \frac{1}{2}\gamma\hat{y}^2,\ \hat{N} = -\frac{b}{c},\ \hat{T} = 0,\ \text{as } \hat{y} \to \infty. \tag{25}$$

Here, $\gamma = \frac{b}{c}$ measures flow obliqueness. The stream function is expressed as [8]

$$\psi(\hat{x}, \hat{y}) = \hat{x}F(\hat{y}) + G(\hat{y}),\ \hat{N}(\hat{x}, \hat{y}) = \hat{x}J(\hat{y}) + S(\hat{y}) \text{ and } \hat{T}(\hat{x}, \hat{y}) = \theta(\hat{y}). \tag{26}$$

Here $F(\hat{y})$, $G(\hat{y})$ and $J(\hat{y})$, $S(\hat{y})$ are defined and as transverse and shear components for flow and micro-rotation respectively. Using equation (26) in (21)–(23), we attain:

$$\frac{\hat{\rho}_f}{\hat{\rho}_{\rm nf}}(1 + A\phi + B\phi^2 + K)F''' + \frac{\hat{\rho}_f}{\hat{\rho}_{\rm nf}}KJ' + FF'' - (F')^2 + C_1 = 0, \tag{27}$$

$$\frac{\hat{\rho}_f}{\hat{\rho}_{\rm nf}}(1 + A\phi + B\phi^2 + K)G''' + \frac{\hat{\rho}_f}{\hat{\rho}_{\rm nf}}KS' + FG'' - F'G' + C_2 = 0, \tag{28}$$

$$\left(1 + A\phi + B\phi^2 + \frac{K}{2}\right)J'' - K(2J + F'') + \frac{\hat{\rho}_{\rm nf}}{\hat{\rho}_f}(FJ' - F'J) = 0, \tag{29}$$

$$\left(1 + A\phi + B\phi^2 + \frac{K}{2}\right)S'' - K(2S + G'') + \frac{\hat{\rho}_{\rm nf}}{\hat{\rho}_f}(FS' - G'J) = 0, \tag{30}$$

$$\frac{\hat{k}_{\rm nf}}{\hat{k}_f}\theta'' + Pr\left(1 - \phi + \frac{(\hat{\rho}c_{\hat{p}})_s}{(\hat{\rho}c_{\hat{p}})_f}\phi\right)F\theta' = 0. \tag{31}$$

In which C_1 and C_2 are integration constant. The reduced boundary conditions become

$$\left.\begin{aligned} &F(0) = 0,\ F'(0) = 1,\ -nF''(0) = J(0),\\ &-nG''(0) = S(0),\ \theta(0) = 1\\ &F'(\infty) = \frac{a}{c},\ G''(\infty) = \gamma,\\ &J(\infty) = 0,\ S(\infty) = -\frac{b}{c},\ \theta(\infty) = 0 \end{aligned}\right\}. \tag{32}$$

Utilizing equation (26) as $F'(\infty)=\frac{a}{c}$ we get $C_1=\left(\frac{a}{c}\right)^2$. $F(\hat{y})=\left(\frac{a}{c}\right)\hat{y}+C$ is obtained by analyzing the boundary layer equation (27) when $\hat{y}\to\infty$, where C describes boundary layer displacement. Similarly using $G''(\infty)=\gamma$, we get $C_2=-C\gamma$. Thus, equations (27) and (28) become

$$(1+A\phi+B\phi^2+K)F'''+KJ'+\frac{\hat{\rho}_{\rm nf}}{\hat{\rho}_f}\times\left(FF''-(F')^2+\left(\frac{a}{c}\right)^2\right)=0, \tag{33}$$

$$(1+A\phi+B\phi^2+K)G'''+KS'+\frac{\hat{\rho}_{\rm nf}}{\hat{\rho}_f}\times(FG''-F'G'-A\gamma)=0. \tag{34}$$

Taking into the account following relation

$$G'(\hat{y})=\gamma H(\hat{y}). \tag{35}$$

Using equation (35) in equations (28) and (34)

$$(1+A\phi+B\phi^2+K)H''+\frac{K}{\gamma}S'+\frac{\hat{\rho}_{\rm nf}}{\hat{\rho}_f}(FH'-F'H-C), \tag{36}$$

$$\left(1+A\phi+B\phi^2+\frac{K}{2}\right)S''-K(2S+\gamma H')+\frac{\hat{\rho}_{\rm nf}}{\hat{\rho}_f}\times(FS'-\gamma HJ)=0. \tag{37}$$

With conditions

$$H(0)=0,\ H'(\infty)=1. \tag{38}$$

Expressions for shear stress and heat transfer rate at the surface are defined as $\hat{\tau}^*{}_{\omega}=\left[(\hat{\mu}_{\rm nf}+\hat{k})\frac{\partial\hat{u}^*}{\partial\hat{y}^*}+\hat{k}\hat{N}^*\right]_{\hat{y}^*=0}$ and $\hat{q}^*{}_{\omega}=-\hat{k}_{\rm nf}\left(\frac{\partial\hat{T}^*}{\partial\hat{y}^*}\right)_{\hat{y}^*=0}$. Non-dimensional form gives

$$\hat{\tau}_{\omega}=(1+A\phi+B\phi^2+K(1-n))(xF''(0)+\gamma H'(0)), \tag{39}$$

$$\hat{q}_{\omega}=-\left(\frac{\hat{k}_{\rm nf}}{\hat{k}_f}\right)\theta'(0). \tag{40}$$

3. Computational procedure using Keller box algorithm

The system of equations (33), (36) (29), (37) and (31) is transported to the first order nonlinear equations by considering

$$F'=U,\ F''=U'=V,\ J'=w,\ H'=t,\ s'=z,\ \theta'=Y\}. \tag{41}$$

Such that equations (33), (36), (29), (37) and (31) becomes

$$(1+A\phi+B\phi^2+K)V'+Kw+\frac{\hat{\rho}_{\rm nf}}{\hat{\rho}_f}\times\left(FV+U^2+\left(\frac{a}{c}\right)^2\right)=0, \tag{42}$$

$$(1+A\phi+B\phi^2+K)t'+\frac{K}{\gamma}z+\frac{\hat{\rho}_{\rm nf}}{\hat{\rho}_f}(Ft-HU-C)=0, \tag{43}$$

$$\left(1+A\phi+B\phi^2+\frac{K}{2}\right)w'-K(2J+V)+\frac{\hat{\rho}_{\rm nf}}{\hat{\rho}_f}\times(Fw-UJ)=0, \tag{44}$$

$$\left(1+A\phi+B\phi^2+\frac{K}{2}\right)z'-K(2s+\gamma t)+\frac{\hat{\rho}_{\rm nf}}{\hat{\rho}_f}\times(Fz-\gamma H)=0, \tag{45}$$

$$\frac{\hat{k}_{\rm nf}}{\hat{k}_f}Y'+Pr\left(1-\phi+\frac{(\hat{\rho}c_{\hat{p}})_s}{(\hat{\rho}c_{\hat{p}})_f}\phi\right)FY=0, \tag{46}$$

and boundary conditions take the form

$$\left.\begin{aligned}&F(0)=0,\ U(0)=1,\ H(0)=0,\ J(0)=-nV(0),\\&s(0)=-n\gamma t(0),\ \theta(0)=1,\\&U(\infty)=\frac{a}{c},\ J(\infty)=0,\ s(\infty)=-\frac{b}{c},\ \theta(\infty)=0,\\&t(\infty)=1.\end{aligned}\right\} \tag{47}$$

The domain is discretized as

$$\eta_0=0,\ \eta_j=\eta_{j-1}+h_j,\ j=1,\ 2,\cdots,J,\ \eta_J=\eta_{\infty}\}. \tag{48}$$

Central difference formulas and the corresponding discretized form of equations (41)–(46) is

$$\left.\begin{aligned}&\frac{(F_j-F_{j-1})}{h_j}=U_{j-\frac{1}{2}},\ \frac{(U_j-U_{j-1})}{h_j}=V_{j-\frac{1}{2}},\\&\frac{(J_j-J_{j-1})}{h_j}=w_{j-\frac{1}{2}},\\&\frac{(H_j-H_{j-1})}{h_j}=t_{j-1/2},\ \frac{(s_j-s_{j-1})}{h_j}=z_{j-1/2},\\&\frac{(\theta_j-\theta_{j-1})}{h_j}=Y_{j-1/2},\end{aligned}\right\}, \tag{49}$$

$$(1+A\phi+B\phi^2+K)(V_j-V_{j-1})h_j^{-1}+Kw_{j-1/2}+\frac{\hat{\rho}_{\rm nf}}{\hat{\rho}_f}\times\left(F_{j-1/2}V_{j-1/2}+U_{j-1/2}^2+\left(\frac{a}{c}\right)^2\right)=0, \tag{50}$$

$$(1+A\phi+B\phi^2+K)(t_j-t_{j-1})h_j^{-1}+\frac{K}{\gamma}z_{j-1/2}+\frac{\hat{\rho}_{\rm nf}}{\hat{\rho}_f}\times(F_{j-1/2}t_{j-1/2}-H_{j-\frac{1}{2}}U_{j-1/2}-C)=0, \tag{51}$$

$$\left(1 + A\phi + B\phi^2 + \frac{K}{2}\right)(w_j - w_{j-1})h_j^{-1} - K \times (2J_{j-\frac{1}{2}} + V_{j-\frac{1}{2}}) + \frac{\hat{\rho}_{\rm nf}}{\hat{\rho}_f}(F_{j-\frac{1}{2}}w_{j-\frac{1}{2}} - U_{j-\frac{1}{2}}J_{j-\frac{1}{2}}) = 0, \tag{52}$$

$$\left(1 + A\phi + B\phi^2 + \frac{K}{2}\right)(z_j - z_{j-1})h_j^{-1} - K(2s_{j-\frac{1}{2}} + \gamma t_{j-\frac{1}{2}}) + \frac{\hat{\rho}_{\rm nf}}{\hat{\rho}_f}(F_{j-\frac{1}{2}}z_{j-\frac{1}{2}} - \gamma H_{j-\frac{1}{2}}) = 0, \tag{53}$$

$$\frac{\hat{k}_{\rm nf}}{\hat{k}_f}(Y_j - Y_{j-1})h_j^{-1} + Pr\left(1 - \phi + \frac{(\hat{\rho}c_{\hat{p}})_s}{(\hat{\rho}c_{\hat{p}})_f}\phi\right)F_{j-1/2}Y_{j-1/2} = 0. \tag{54}$$

Equations (49)–(54) are nonlinear algebraic equations and can be linearized by using Newton iterations as follows:

For $(i+1)$th iterates

$$F_j^{i+1} = F_j^i + \delta F_j^i, \text{ etc} \tag{55}$$

for all dependent variables. Using these expressions in equations (49)–(54) and keeping linear terms in δF_j^i, etc, a linear tri-diagonal system is acquired as follow

$$\left.\begin{aligned}
&\delta F_j - \delta F_{j-1} - \frac{h_j}{2}(\delta \mathrm{U}_j - \delta U_{j-1}) = (r_1)_{j-\frac{1}{2}}\\
&\delta \mathrm{U}_j - \delta \mathrm{U}_{j-1} - \frac{h_j}{2}(\delta \mathrm{V}_j - \delta V_{j-1}) = (r_2)_{j-\frac{1}{2}}\\
&\delta J_j - \delta J_{j-1} - \frac{h_j}{2}(\delta w_j - \delta w_{j-1}) = (r_3)_{j-\frac{1}{2}}\\
&\delta H_j - \delta H_{j-1} - \frac{h_j}{2}(\delta t_j - \delta t_{j-1}) = (r_4)_{j-\frac{1}{2}}\\
&\delta s_j - \delta s_{j-1} - \frac{h_j}{2}(\delta z_j - \delta z_{j-1}) = (r_5)_{j-\frac{1}{2}}\\
&\delta \theta_j - \delta \theta_{j-1} - \frac{h_j}{2}(\delta Y_j - \delta Y_{j-1}) = (r_6)_{j-\frac{1}{2}}
\end{aligned}\right\}, \tag{56}$$

$$\left.\begin{aligned}
&(\xi_1)_j\delta V_j - (\xi_2)_j\delta V_{j-1} + C_2\delta w_j + C_2\delta w_{j-1} + (\xi_3)_j\delta F_j + (\xi_3)_j\delta F_{j-1} - (\xi_4)_j\delta U_j - (\xi_4)_j\delta U_{j-1} = (r_7)_j\\
&(\xi_1)_j\delta t_j - (\xi_2)_j\delta t_{j-1} + C_4\delta z_j + C_4\delta z_{j-1} + (\xi_5)_j\delta F_j + (\xi_5)_j\delta F_{j-1} - (\xi_6)_j\delta U_j - (\xi_6)_j\delta U_{j-1} - (\xi_7)_j\delta \mathrm{H}_j - (\xi_7)_j\delta \mathrm{H}_{j-1} = (r_8)_j\\
&(\xi_8)_j\delta w_j - (\xi_9)_j\delta w_{j-1} - (C_2 + (\xi_7)_j)\delta J_j - (C_2 + (\xi_7)_j)\delta J_{j-1} - \frac{K}{2}\delta V_j - \frac{K}{2}\delta V_{j-1} + (\xi_{10})_j\delta F_j + (\xi_{10})_j\delta F_{j-1} - (\xi_{11})_j\delta U_j - (\xi_{11})_j\delta U_{j-1} = (r_9)_j\\
&(\xi_8)_j\delta z_j - (\xi_9)_j\delta z_{j-1} - 2C_2\delta s_j - 2C_2\delta s_{j-1} - \gamma C_2\delta t_j - \gamma C_2\delta t_{j-1} + (\xi_{12})_j\delta F_j + (\xi_{12})_j\delta F_{j-1} - 2\gamma\, C_3\delta H_j - 2\gamma\, C_3\delta \mathrm{H}_{j-1} = (r_{10})_j\\
&(\xi_{13})_j\delta Y_j - (\xi_{14})_j\delta Y_{j-1} + (\xi_{15})_j\delta F_j + (\xi_{15})_j\delta F_{j-1} = (r_{11})_j
\end{aligned}\right\}. \tag{57}$$

With

$$\left.\begin{aligned}
&\delta F_0(0) = 0,\ \delta U_0(0) = 0,\ \delta H_0(0) = 0,\\
&\delta J_0(0) = -n\delta V_0(0),\ \ \delta s_0(0) = -n\gamma\delta t_0(0),\\
&\delta\theta_0(0) = 0,\ \delta U_J = 0,\ \delta J_J = 0,\\
&\delta s_J = 0,\ \ \delta\theta_J = 0,\ \delta t_J = 0.
\end{aligned}\right\}, \tag{58}$$

where

$$\left.\begin{aligned}
&a_j = \frac{h_j}{2},\ C_1 = 1 + A\phi + B\phi^2 + K,\ C_2 = \frac{Kh_j}{2},\ C_3 = \frac{h_j}{4}\frac{\hat{\rho}_{\rm nf}}{\hat{\rho}_f},\\
&C_4 = \frac{Kh_j}{2\gamma},\ C_5 = 1 + A\phi + B\phi^2 + \frac{K}{2},\\
&(\xi_1)_j = C_1 + C_3(F_j + F_{j-1}),\ (\xi_2)_j = C_1 - C_3(F_j + F_{j-1}),\\
&(\xi_3)_j = C_3(V_j + V_{j-1}),\ (\xi_4)_j = 2C_3(U_j + U_{j-1}),\\
&(\xi_5)_j = C_3(t_j + t_{j-1}),\ (\xi_6)_j = C_3(H_j + H_{j-1}),\\
&(\xi_7)_j = C_3(U_j + U_{j-1}),\ (\xi_8)_j = C_5 + C_3(F_j + F_{j-1}),\\
&(\xi_9)_j = C_5 - C_3(F_j + F_{j-1}),\ (\xi_{10})_j = C_3(w_j + w_{j-1}),\\
&(\xi_{11})_j = C_3(J_j + J_{j-1}),\ (\xi_{12})_j = C_3(z_j + z_{j-1}),\\
&(\xi_{13})_j = \frac{\hat{k}_{\rm nf}}{\hat{k}_f} + \frac{Prh_j}{4}\left(1 - \phi + \frac{(\hat{\rho}c_{\hat{p}})_s}{(\hat{\rho}c_{\hat{p}})_f}\phi\right)(F_j + F_{j-1}),\\
&(\xi_{14})_j = \frac{\hat{k}_{\rm nf}}{\hat{k}_f} - \frac{Prh_j}{4}\left(1 - \phi + \frac{(\hat{\rho}c_{\hat{p}})_s}{(\hat{\rho}c_{\hat{p}})_f}\phi\right)(F_j + F_{j-1}),\\
&(\xi_{15})_j = \frac{Prh_j}{4}\left(1 - \phi + \frac{(\hat{\rho}c_{\hat{p}})_s}{(\hat{\rho}c_{\hat{p}})_f}\phi\right)(Y_j + Y_{j-1}),\\
&(r_1)_j = F_{j-1} - F_j + h_jU_{j-\frac{1}{2}},\ (r_2)_j = U_{j-1} - U_j + h_jV_{j-\frac{1}{2}},\\
&(r_3)_j = J_{j-1} - J_j + h_jw_{j-\frac{1}{2}},\ (r_4)_j = H_{j-1} - H_j + h_jt_{j-\frac{1}{2}},\\
&(r_5)_j = s_{j-1} - s_j + h_jz_{j-\frac{1}{2}},\ (r_6)_j = \theta_{j-1} - \theta_j + h_jY_{j-\frac{1}{2}},\\
&(r_7)_j = C_1(V_{j-1} - V_j) + C_2(w_j + w_{j-1})\\
&-C_3\left\{(F_j + F_{j-1})(V_j + V_{j-1}) - U_j^2 - U_{j-1}^2 - \left(\frac{2a}{\mathrm{c}}\right)^2\right\},\\
&(r_8)_j = C_1(t_{j-1} - t_j) + C_4(z_j + z_{j-1})\\
&-C_3\{(F_j + F_{j-1})(t_j + t_{j-1}) - (U_j + U_{j-1})(H_j + H_{j-1}) - 4A\},\\
&(r_9)_j = C_5(w_{j-1} - w_j) + C_2(J_j + J_{j-1}) + \frac{K}{2}(U_j - U_{j-1})\\
&-C_3\{(F_j + F_{j-1})(w_j + w_{j-1}) - (U_j + U_{j-1})(J_j + J_{j-1})\},\\
&(r_{10})_j = C_5(z_{j-1} - z_j) + 2C_2(s_j + s_{j-1}) + \gamma C_2(t_j - t_{j-1})\\
&-C_3\{(F_j + F_{j-1})(z_j + z_{j-1}) - 2\gamma(H_j + H_{j-1})\},\\
&(r_{11})_j = \frac{\hat{k}_{\rm nf}}{\hat{k}_f}(Y_{j-1} - Y_j) - (\xi_{15})_j\{(F_j + F_{j-1})(J_j + J_{j-1})\},
\end{aligned}\right\}. \tag{59}$$

Linearized equations from (56) to (57) in vector form are:

$$A\delta = r, \tag{60}$$

where

$$A = \begin{bmatrix}
[A_1] & [E_1] & & & & & \\
[B_2] & [A_2] & [C_2] & & & & \\
 & & \ddots & & & & \\
 & & & \ddots & & & \\
 & & & & \cdot & [B_{J-1}] & [A_{J-1}] & [C_{J-1}]\\
 & & & & & [B_J] & [A_J]
\end{bmatrix}$$

$$\delta = \begin{bmatrix} [\delta_1] \\ [\delta_2] \\ \vdots \\ \vdots \\ \vdots \\ [\delta_{J-1}] \\ [\delta_J] \end{bmatrix}, \quad r = \begin{bmatrix} [r_1] \\ [r_2] \\ \vdots \\ \vdots \\ \vdots \\ [r_{J-1}] \\ [r_J] \end{bmatrix}$$

$$A_1 = \begin{bmatrix} 0 & 0 & 0 & 0 & 0 & 1 & 0 & 0 & 0 & 0 & 0 \\ -a_1 & 0 & 0 & 0 & 0 & 0 & -a_1 & 0 & 0 & 0 & 0 \\ 0 & -a_1 & 0 & 0 & 0 & 0 & 0 & -a_1 & 0 & 0 & 0 \\ 0 & 0 & -a_1 & 0 & 0 & 0 & 0 & 0 & -a_1 & 0 & 0 \\ 0 & 0 & 0 & -a_1 & 0 & 0 & 0 & 0 & 0 & -a_1 & 0 \\ 0 & 0 & 0 & 0 & -a_1 & 0 & 0 & 0 & 0 & 0 & -a_1 \\ -(\xi_2)_1 & C_2 & 0 & 0 & 0 & (\xi_3)_1 & (\xi_1)_1 & C_2 & 0 & 0 & 0 \\ 0 & 0 & -(\xi_2)_1 & C_4 & 0 & (\xi_5)_1 & 0 & 0 & (\xi_1)_1 & C_4 & 0 \\ \frac{K}{2} & -(\xi_9)_1 & 0 & 0 & 0 & (\xi_{10})_1 & \frac{K}{2} & (\xi_8)_1 & 0 & 0 & 0 \\ 0 & 0 & -K\gamma a_1 & -(\xi_9)_1 & 0 & (\xi_{12})_1 & 0 & 0 & -K\gamma a_1 & (\xi_8)_1 & 0 \\ 0 & 0 & 0 & 0 & -(\xi_{14})_1 & (\xi_{15})_1 & 0 & 0 & 0 & 0 & (\xi_{13})_1 \end{bmatrix}$$

$$A_j = \begin{bmatrix} -a_j & 0 & 0 & 0 & 0 & 1 & 0 & 0 & 0 & 0 & 0 \\ -1 & 0 & 0 & 0 & 0 & 0 & -a_j & 0 & 0 & 0 & 0 \\ 0 & -1 & 0 & 0 & 0 & 0 & 0 & -a_j & 0 & 0 & 0 \\ 0 & 0 & -1 & 0 & 0 & 0 & 0 & 0 & -a_j & 0 & 0 \\ 0 & 0 & 0 & -1 & 0 & 0 & 0 & 0 & 0 & -a_j & 0 \\ 0 & 0 & 0 & 0 & -1 & 0 & 0 & 0 & 0 & 0 & -a_j \\ -(\xi_4)_j & 0 & 0 & 0 & 0 & (\xi_3)_j & (\xi_1)_j & C_2 & 0 & 0 & 0 \\ -(\xi_6)_j & 0 & -(\xi_7)_j & 0 & 0 & (\xi_5)_j & 0 & 0 & (\xi_1)_j & C_4 & 0 \\ -(\xi_{11})_j & -Ka_j - (\xi_7)_j & 0 & 0 & 0 & (\xi_{10})_j & \frac{K}{2} & (\xi_8)_j & 0 & 0 & 0 \\ 0 & 0 & -2\gamma C_3 & -2ka_j & 0 & (\xi_{12})_j & 0 & 0 & -K\gamma a_j & (\xi_8)_j & 0 \\ 0 & 0 & 0 & 0 & 0 & (\xi_{15})_j & 0 & 0 & 0 & 0 & (\xi_{13})_j \end{bmatrix},$$

$$2 \leqslant j \leqslant J$$

$$B_j = \begin{bmatrix} 0 & 0 & 0 & 0 & 0 & 1 & 0 & 0 & 0 & 0 & 0 \\ 0 & 0 & 0 & 0 & 0 & 0 & -a_j & 0 & 0 & 0 & 0 \\ 0 & 0 & 0 & 0 & 0 & 0 & 0 & -a_j & 0 & 0 & 0 \\ 0 & 0 & 0 & 0 & 0 & 0 & 0 & 0 & -a_j & 0 & 0 \\ 0 & 0 & 0 & 0 & 0 & 0 & 0 & 0 & 0 & -a_j & 0 \\ 0 & 0 & 0 & 0 & 0 & 0 & 0 & 0 & 0 & 0 & -a_j \\ 0 & 0 & 0 & 0 & 0 & (\xi_3)_1 & -(\xi_2)_j & C_2 & 0 & 0 & 0 \\ 0 & 0 & 0 & 0 & 0 & (\xi_5)_1 & 0 & 0 & -(\xi_2)_j & C_4 & 0 \\ 0 & 0 & 0 & 0 & 0 & (\xi_{10})_1 & \frac{K}{2} & -(\xi_9)_j & 0 & 0 & 0 \\ 0 & 0 & 0 & 0 & 0 & (\xi_{12})_1 & 0 & 0 & -K\gamma a_j & -(\xi_9)_j & 0 \\ 0 & 0 & 0 & 0 & 0 & (\xi_{15})_1 & 0 & 0 & 0 & 0 & -(\xi_{14})_j \end{bmatrix},$$

$$2 \leqslant j \leqslant J$$

$$E_j = \begin{bmatrix} -a_j & 0 & 0 & 0 & 0 & 0 & 0 & 0 & 0 & 0 & 0 \\ 1 & 0 & 0 & 0 & 0 & 0 & 0 & 0 & 0 & 0 & 0 \\ 0 & 1 & 0 & 0 & 0 & 0 & 0 & 0 & 0 & 0 & 0 \\ 0 & 0 & 1 & 0 & 0 & 0 & 0 & 0 & 0 & 0 & 0 \\ 0 & 0 & 0 & 1 & 0 & 0 & 0 & 0 & 0 & 0 & 0 \\ 0 & 0 & 0 & 0 & 1 & 0 & 0 & 0 & 0 & 0 & 0 \\ -(\xi_4)_j & 0 & 0 & 0 & 0 & 0 & 0 & 0 & 0 & 0 & 0 \\ -(\xi_6)_j & 0 & -(\xi_7)_j & 0 & 0 & 0 & 0 & 0 & 0 & 0 & 0 \\ -(\xi_{11})_j & -Ka_j - (\xi_7)_j & 0 & 0 & 0 & 0 & 0 & 0 & 0 & 0 & 0 \\ 0 & 0 & -2\gamma C_3 & -2Ka_j & 0 & 0 & 0 & 0 & 0 & 0 & 0 \\ 0 & 0 & 0 & 0 & 0 & 0 & 0 & 0 & 0 & 0 & 0 \end{bmatrix},$$

$$2 \leqslant j \leqslant J$$

$$[\delta_1] = \begin{bmatrix} \delta V_0 \\ \delta w_0 \\ \delta t_0 \\ \delta z_0 \\ \delta Y_0 \\ \delta f_1 \\ \delta V_1 \\ \delta w_1 \\ \delta t_1 \\ \delta z_1 \\ \delta Y_1 \end{bmatrix}, [\delta_j] = \begin{bmatrix} \delta U_{j-1} \\ \delta J_{j-1} \\ \delta H_{j-1} \\ \delta S_{j-1} \\ \delta \theta_{j-1} \\ \delta F_j \\ \delta V_j \\ \delta w_j \\ \delta t_j \\ \delta z_j \\ \delta Y_j \end{bmatrix},$$

$$2 \leqslant j \leqslant J,\ [r_j] = \begin{bmatrix} (r_1)_{j-1/2} \\ (r_2)_{j-1/2} \\ (r_3)_{j-1/2} \\ (r_4)_{j-1/2} \\ (r_5)_{j-1/2} \\ (r_6)_{j-1/2} \\ (r_7)_{j-1/2} \\ (r_8)_{j-1/2} \\ (r_9)_{j-1/2} \\ (r_{10})_{j-1/2} \\ (r_{11})_{j-1/2} \end{bmatrix} 1 \leqslant j \leqslant J.$$

Consider

$$A = Lu, \tag{61}$$

where

$$L = \begin{bmatrix} [\alpha_1] & & & & \\ [B_2] & [\alpha_2] & & & \\ & \ddots & \ddots & & \\ & & \ddots & [\alpha_{J-1}] & \\ & & & [B_J] & [\alpha_J] \end{bmatrix}.$$

And

$$u = \begin{bmatrix} [I] & [\Gamma_1] & & & & \\ & [I] & [\Gamma_2] & & & \\ & & \ddots & & & \\ & & \ddots & \ddots & & \\ & & & \ddots & & \\ & & & & [I] & [\Gamma_{J-1}] \\ & & & & & [I] \end{bmatrix}.$$

Here $[I]$ is unit matrix and $[\alpha_i], [\Gamma_i]$ are square matrices of order 11 whose elements are determined by following expressions:

$$[\alpha_1] = [A_1],\ [A_1][\Gamma_1] = [C_1],\ [\alpha_j] = [A_j] - [B_j][\Gamma_{j-1}],\ j = 2, 3, ..., J,\ [\alpha_j][\Gamma_j] = [C_j],\ j = 2, 3, ..., J-1$$

Incorporating equation (61) into (60) yields

$$LU\delta = r.$$

Let

$$U\delta = W. \tag{62}$$

So that

$$LW = r.$$

In which

$$W = \begin{bmatrix} [W_1] \\ [W_2] \\ [W_3] \\ [W_4] \\ [W_5] \\ [W_6] \\ [W_7] \\ [W_8] \\ [W_9] \\ [W_{10}] \\ [W_{11}] \end{bmatrix},$$

And $[W_j]$ is an 11×1 column matrix. Elements of W are solved from following equations

$$[\alpha_1][W_1] = [r_1],$$
$$[\alpha_j][W_j] = [r_j] - [B_j][W_{j-1}],$$

Γ_j, α_j and W_j are calculated by forward sweep. Once the elements of W are computed, equation (62) gives the solution δ whose elements are attained from subsequent relations:

$$[\delta_J] = [W_J],$$
$$[\delta_j] = [W_j] - [\Gamma_j][\delta_{j+1}],\ j = 2, 3, ..., J$$

These calculations are performed until iterative error becomes less than 10^{-6}.

4. Results and discussion

Different shape effects of MoS_2 nanoparticles suspended in water based oblique micropolar nanofluid has been studied

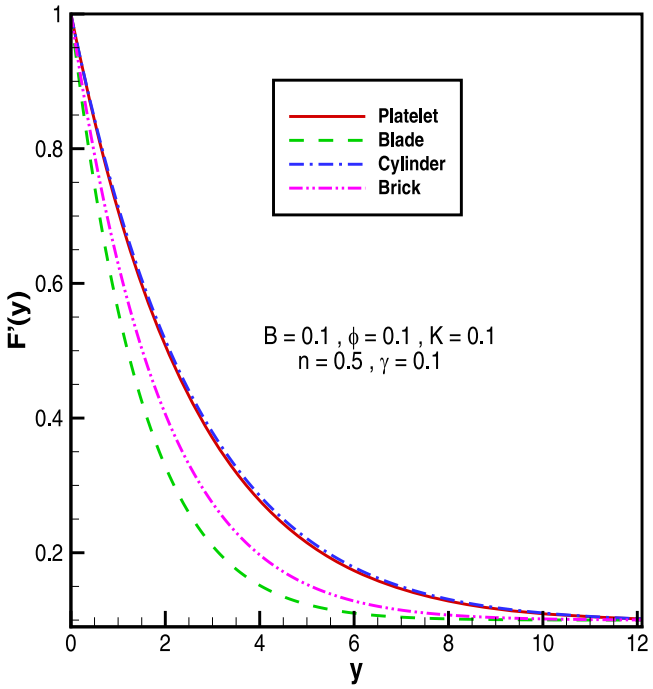

Figure 2. Various shape effects of MoS_2 nanoparticles on normal velocity profile $F'(y)$.

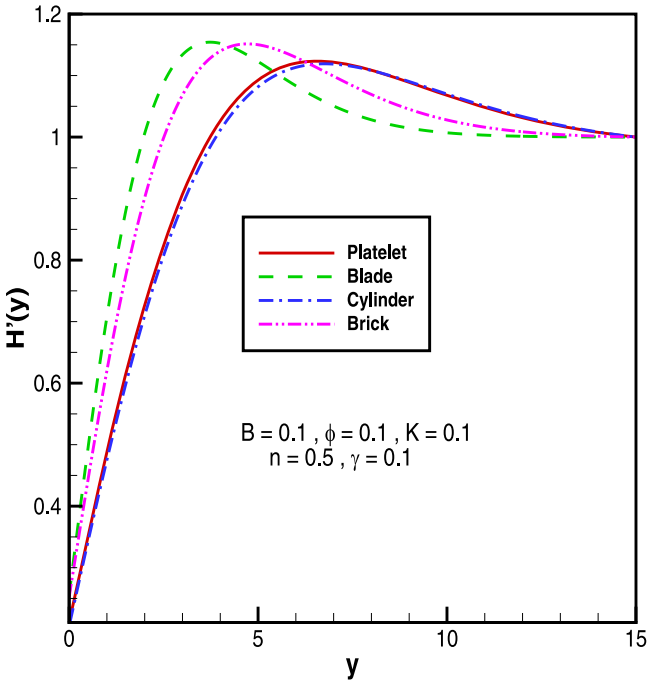

Figure 3. Various shape effects of MoS_2 nanoparticles on tangential velocity profile $H'(y)$.

Table 3. Thermal characteristics of water and Molybdenum disulfide [4].

Thermo-physical properties	$\hat{\rho}$(kg m^{-3})	$c_{\hat{p}}$(J kg^{-1} K^{-1})	$\hat{k}$(W m^{-1} k^{-1})
H_2O	997.1	4179	0.613
MoS_2	5.06×10^3	397.21	904.4

numerically. Four distinct shapes of MoS_2 nanoparticles called, platelet, cylinder, brick and blade are explored for some appropriate fixed values of rest of the pertinent parameters, namely, stretching ratio B, nanosized particles volume fraction ϕ, material constant K, microelement concentration n, obliqueness parameter γ are used in calculations.Thermal characteristics of water and Molybdenum disulfide are presented in Table 3. Keller Box method is engaged to attain the numerical results [30]. Graphs of flow characteristic such as velocity, temperature, micro-rotation; thermal conductivity, skin friction coefficient and local heat flux developed by numerical results are displayed in figures 2–12. Figures 2 and 3 show the shape effects of molybdenum disulfide on normal and tangential velocity profiles of the oblique micropolar nanofluid flow. In figure 2 it is noticed that MoS_2 micropolar nanofluid has highest normal velocity profile $F'(y)$ for cylindrical shaped nanoparticles while lowest velocity profile when the blade shaped nanoparticles are inserted. Figure 3 reveals quite opposite flow behavior of tangential velocity profile as compared with normal velocity profile. It is discovered that near the surface flow with bladelike nanoparticles has maximum tangential velocity profile $H'(y)$ and flow with cylinder like nanoparticles has lowest velocity profile but away from the surface reverse behavior is observed. In figure 4 maximum

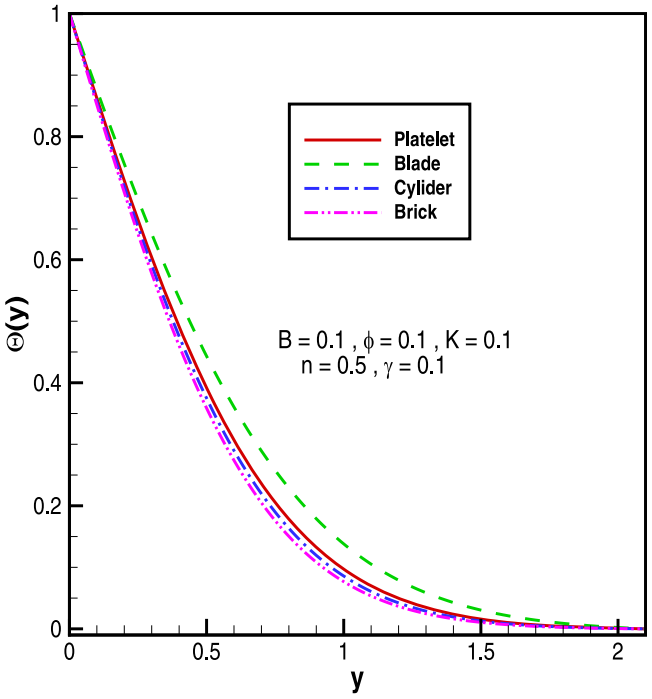

Figure 4. Various shape effects of MoS_2 nanoparticles on temperature profile $\theta(y)$.

temperature distribution $\theta(y)$ is noticed with blade shaped nanoparticles but flow with brick shaped nanoparticles noticed with lowest temperature distribution. Micro-rotation profile of micropolar nanofluid with insertion of diverse shapes of nanoparticles is presented in figure 5 for fixed value $\hat{x} = 1$. It is witnessed that near the surface flow with blade like nanoparticles has maximum micro-rotation profile but lowest micro-rotation

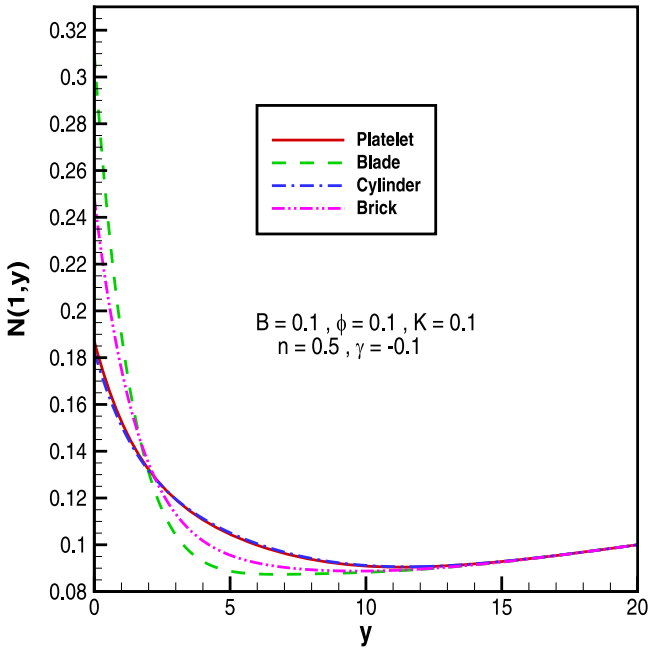

Figure 5. Various shape effectsof MoS_2 nanoparticles on micro-rotation profile with $\hat{x} = 1$.

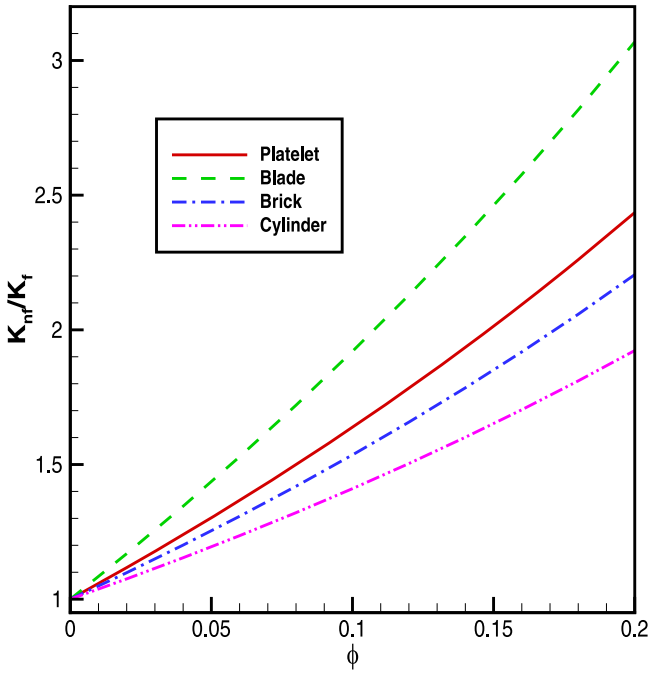

Figure 6. Shape effects of MoS_2 nanoparticles on thermal conductivity of micropolar nanofluid.

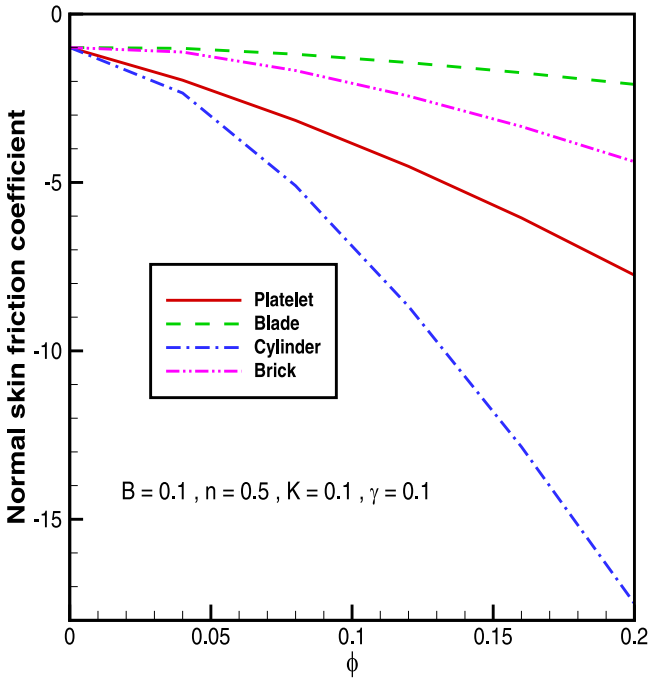

Figure 7. Normal skin friction coefficient $(1 + A\phi + B\phi^2 + K(1 - n))F''(0)$ against ϕ.

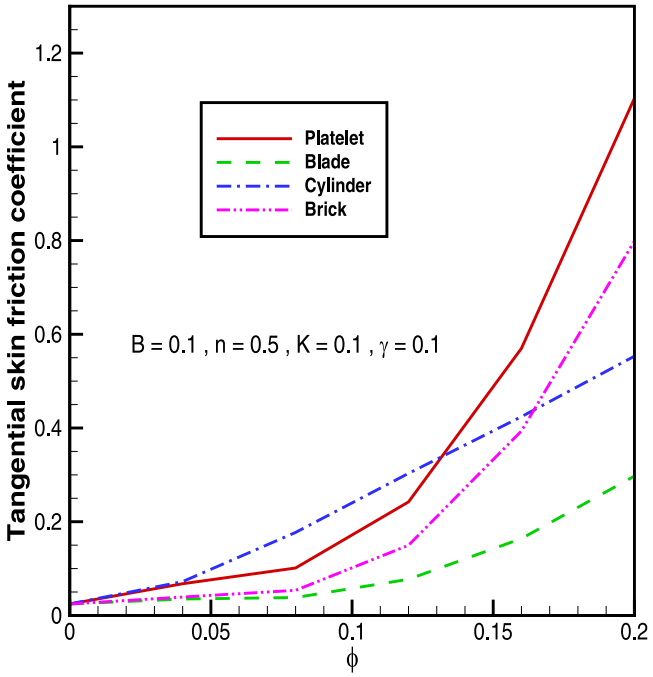

Figure 8. Tangential skin friction coefficient $\gamma(1 + A\phi + B\phi^2 + K(1 - n))H'(0)$ against ϕ.

profile is observed with cylinder like nanoparticles. Enhancement in thermal conductivity, which is defined by the ratio $\frac{\hat{k}_{nf}}{\hat{k}_f}$, against MoS_2 nanoparticles volume fraction ϕ is plotted in figure 6. It is perceived that water based nanofluid thermal conductivity raises with MoS_2 nanoparticles volume fraction. Moreover it is noted that suspension of blade shaped nanoparticles has highest, on the other hand, cylinder like nanoparticles suspension has lowest thermal conductivity ratio. Normal and tangential skin friction coefficient against nanoparticles volume fraction ϕ with various shapes are shown in figures 7 and 8. It is noticed that normal skin friction coefficient $(1 + A\phi + B\phi^2 + K(1 - n))F''(0)$ at the surface decreases while tangential skin friction coefficient $\gamma(1 + A\phi + B\phi^2 + K(1 - n))H'(0)$ increases with growth in molybdenum Disulfide nanoparticles volume fraction. Further it is observed that normal skin friction coefficient at the surface is

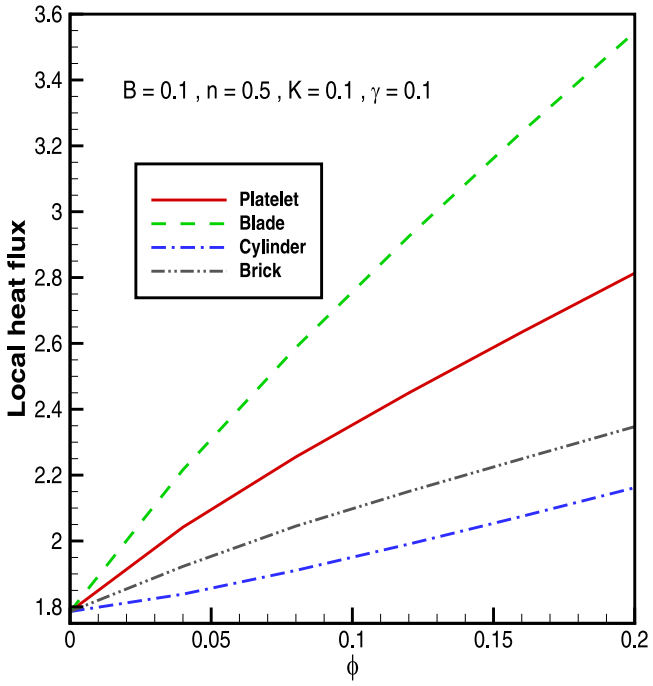

Figure 9. Local heat flux $\hat{q}_{\omega} = -\left(\frac{\hat{k}_{nf}}{\hat{k}_f}\right)\theta'(0)$ against ϕ.

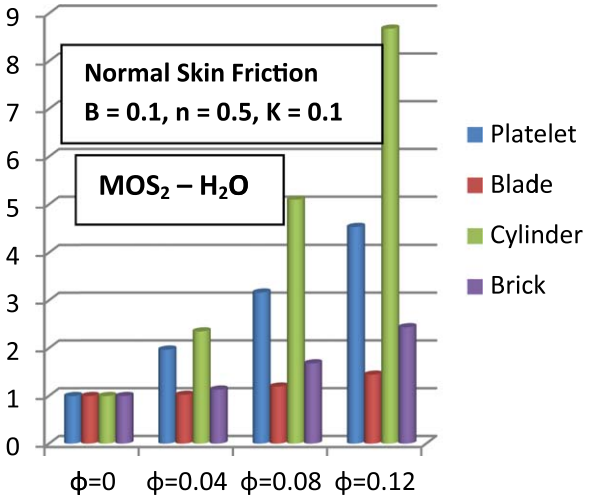

Figure 10. Magnitude of normal skin friction coefficient against nanoparticles volume fraction.

lowest with cylinder like nanoparticles but it is highest with inclusion of blade shaped nanoparticles. Figure 8 shows entirely opposite behavior in tangential skin friction coefficient as compared with normal skin friction coefficient of the flow as it is maximum in presence of cylinder like nanoparticles (near the surface) but lowest with addition of blade shaped nanoparticles. Local heat flux $\hat{q}_{\omega} = -\left(\frac{\hat{k}_{nf}}{\hat{k}_f}\right)\theta'(0)$ of MoS_2 micropolar nanofluid at the surface is plotted against MoS_2 nanoparticles volume fraction ϕ with different shapes is presented in figure 9. It increases linearly with increase in nanoparticles volume fraction. Moreover local heat flux at the surface is highest with blade shaped nanoparticles and lowest with cylinder shaped

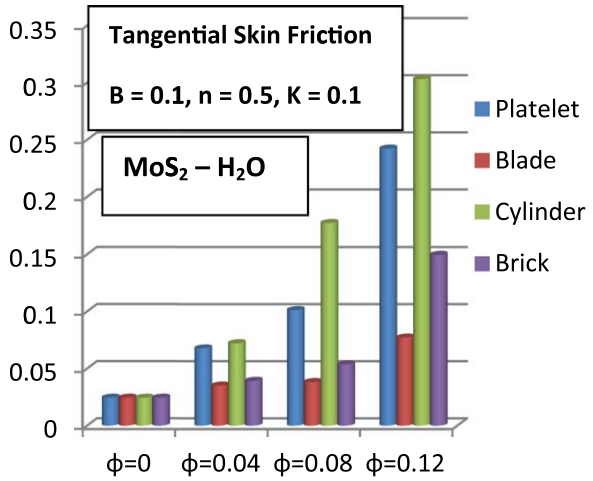

Figure 11. Magnitude of tangential skin friction coefficient against nanoparticles volume fraction.

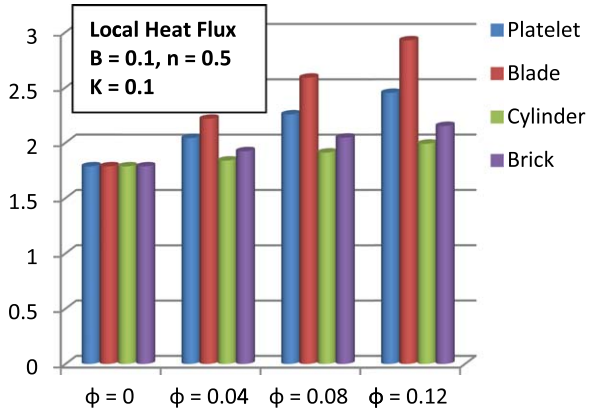

Figure 12. Local heat flux with nanoparticles volume fraction.

nanoparticles. Variation in stresses and heat transfer rate influenced by Molybdenum Disulfide nanoparticles volume fraction with different shapes is shown through bar graphs from figures 10–12. Figure 10 shows that magnitude of normal skin friction coefficient increases by increasing nanoparticles volume fraction of all shapes. Moreover, it is observed that blade shaped nanoparticles offers lowest while nanoparticles of cylindrical shape display highest magnitude of normal skin friction coefficient by increasing their volume fraction. Likewise, irrespective of different shapes, rise in tangential skin friction coefficient magnitude is noticed in figure 11 with volume fraction of nanoparticles. In the same way, blade and cylindrical shaped nanoparticles exhibit lowest and highest magnitude of tangential skin friction when their volume fraction grows respectively. On the contrary, figure 12 depicts highest heat transfer rate with blade shaped whereas lowest rate of heat transfer with cylinder shaped MoS_2 nanoparticles.

5. Concluding remarks

This communication investigates oblique stagnated flow of micropolar nanofluid towards an extending sheet. Various

shape effects of molybdenum Disulfide nanoparticles are studied on flow and heat transfer features. Key discoveries of the investigation are stated that flow with blade like MoS_2 nanoparticles depicts maximum temperature distribution and micro-rotation profile near the surface. Maximum ratio of thermal conductivities $\frac{\hat{k}_{nf}}{\hat{k}_f}$ is gained with inclusion of blade shape MoS_2 nanoparticles. Volume fraction ϕ contributes significantly in decreasing normal skin friction where as it enhances local heat transfer rate. Blade shape nanoparticles exhibited lowest skin friction and highest rate of heat transfer at the surface.

Acknowledgments

The authors extend their appreciation to the Deanship of Scientific Research at King Khalid University, Abha 61413, Saudi Arabia for funding this work through research groups program under grant number R.G.P-2/32/40.

ORCID iDs

M S Alqarni https://orcid.org/0000-0001-8063-4449
M Y Malik https://orcid.org/0000-0002-5301-4145
R Mehmood https://orcid.org/0000-0003-1891-6677

References

[1] Eastman J A and Choi S U S 1995 Enhancing thermal conductivity of fluids with nanoparticles *Conference: 1995 International Mechanical Engineering Congress and Exhibition (San Francisco, CA)*
[2] Timofeeva E V, Routbort J L and Singh D 2009 *J. Appl. Phys.* **106**
[3] Ellahi R, Hassan M and Zeeshan A 2015 *Int. J. Heat Mass Transfer* **81** 449
[4] Shafie S, Gul A and Khan I 2016 *AIP Conf. Proc.* **1775** 030042
[5] Hiemenz K 1911 *Dinglers Polytech. J.* **326** 321
[6] Wang X Q and Mujumdar A S 2007 *Int. J. Therm. Sci.* **46** 1-19
[7] Nadeem S, Mehmood R and Akbar N S 2013 *Int. J. Heat Mass Transfer* **57** 679
[8] Nadeem S, Ijaz S and Akbar N S 2013 *J. Comput. Theor. Nanosci.* **10** 2751
[9] Rashidi M M, Momoniat E, Ferdows M and Basiriparsa A 2014 *Math. Problems Eng.* **2014** 239082
[10] Nadeem S, Mehmood R and Akbar N S 2014 *J. Comput. Theor. Nanosci.* **11** 1422
[11] Abolbashari M H, Freidoonimehr N, Nazari F and Rashidi M M 2015 *Adv. Powder Technol.* **26** 542
[12] Rehman U, Mehmood R and Nadeem S 2017 *Appl. Therm. Eng.* **112** 832
[13] Mehmood R, Nadeem S and Akbar N S 2016 *J. Appl. Fluid Mech.* **9** 1359
[14] Rana S, Mehmood R and Akbar N S 2016 *J. Mol. Liq.* **222** 1010
[15] Eringen C 1966 *J. Math. Fluid Mech.* **16** 1
[16] Nazar R, Amin N, Filip D and Pop I 2004 *Intern. J. Nonlinear Mech.* **39** 1227
[17] Damseh R A, Al-Odata M Q, Chamkha A J and Shannak B A 2009 *Int. J. Therm. Sci.* **48** 1658
[18] Nadeem S, Rehman A, Vajravelu K, Lee J and Lee C 2012 *Math. Problems Eng.* **2012** 640289
[19] Rehman A and Nadeem S 2012 *Chin. Phys. Lett.* **29** 124701
[20] Mahmoud M A A and Waheed S E 2012 *J. Egypt. Math. Soc.* **20** 20
[21] Hussain S T, Nadeem S and Haq R U 2014 *Eur. J. Phys. Plus* **129** 161
[22] Sheikoleslami M, Hatami M and Ganji D D 2014 *J. Mol. Liq.* **194** 30
[23] Noor N F M, Haq R U, Nadeem S and Hashim I 2015 *Meccanica* **50** 2007
[24] Adegbie S K, Koriko O K and Animasaun I L 2016 *J. Nigerian Math. Soc.* **35** 34
[25] Mehmood R, Nadeem S and Masood S 2016 *J. Magn. Magn. Mater.* **401** 1006
[26] Waqas M, Farooq M, Khan M I, Alsaedi A, Hayat T and Yasmeen T 2016 *Int. J. Heat Mass Transfer* **102** 766
[27] Khanafer K, Vafai K and Lightstone M 2003 *Int. J. Heat Mass Transfer* **46** 3639
[28] Hamilton R L and Crosser O K 1962 *Ind. Eng. Chem.* **1** 187
[29] Timofeeva E V, Routbort J L and Singh D 2009 *J. Appl. Phys.* **106** 014304
[30] Meek P C and Norbury J 2006 *SIAM J. Numer. Anal.* **21** 883
[31] Khan W A, Makinde O D and Khan Z H 2016 Non-aligned MHD stagnation point flow of variable viscosity nanofluids past a stretching sheet with radiative heat *Int. J. Heat Mass Transfer* **96** 525
[32] Makinde O D, Khan W A and Khan Z H 2013 Buoyancy effects on MHD stagnation point flow and heat transfer of a nanofluid past a convectively heated stretching/shrinking sheet *Int. J. Heat Mass Transfer* **62** 526
[33] Makinde O D, Khan W A and Khan Z H 2017 Stagnation point flow of MHD chemically reacting nanofluid over a stretching convective surface with slip and radiative heat *Proc. Inst. Mech. Eng.* E **231** 695
[34] Rehman K U, Khan A A, Malik M Y and Makinde O D 2017 Thermophysical aspects of stagnation point magnetonanofluid flow yields by an inclined stretching cylindrical surface: a non-Newtonian fluid model *J. Braz. Soc. Mech. Sci. Eng.* **39** 3669
[35] Ibrahim W and Makinde O D 2016 Magnetohydrodynamic stagnation point flow of a power-law nanofluid towards a convectively heated stretching sheet with slip *Proc. Inst. Mech. Eng.* E **230** 345
[36] Ibrahim W and Makinde O D 2016 Magnetohydrodynamic stagnation point flow and heat transfer of Casson nanofluid past a stretching sheet with slip and convective boundary condition *J. Aerosp. Eng.* **29** 04015037